JACS
JOURNAL OF THE AMERICAN CHEMICAL SOCIETY
Article
pubs.acs.org/JACS

Control of Intrachain Charge Transfer in Model Systems for Block Copolymer Photovoltaic Materials

Kerr Johnson,[†] Ya-Shih Huang,[†] Sven Huettner,[†] Michael Sommer,[‡,#] Martin Brinkmann,[∥] Rhiannon Mulherin,[†] Dorota Niedzialek,[§] David Beljonne,[§] Jenny Clark,[†] Wilhelm T. S. Huck,[‡,⊥] and Richard H. Friend*[,†]

[†]Cavendish Laboratory, University of Cambridge, J. J. Thomson Avenue, Cambridge CB3 0HE, United Kingdom
[‡]Melville Laboratory for Polymer Synthesis, Lensfield Road, Cambridge CB2 1EW, United Kingdom
[§]Laboratory for Chemistry of Novel Materials, Université de Mons, Place du Parc, 20, 7000 Mons, Belgium
[∥]Institut Charles Sadron, 6 Rue Boussingault, 67083 Strasbourg, France
[⊥]Institute for Molecules and Materials, Radboud University Nijmegen, Heyendaalseweg, 135 6525 AJ Nijmegen, The Netherlands

Supporting Information

ABSTRACT: We report the electronic properties of the conjugated coupling between a donor polymer and an acceptor segment serving as a model for the coupling in conjugated donor−acceptor block copolymers. These structures allow the study of possible intrachain photoinduced charge separation, in contrast to the interchain separation achieved in conventional donor−acceptor blends. Depending on the nature of the conjugated linkage, we observe varying degrees of modification of the excited states, including the formation of intrachain charge transfer excitons. The polymers comprise a block (typically 18 repeat units) of P3HT, poly(3-hexyl thiophene), coupled to a single unit of F8-TBT (where F8 is dioctylfluorene, and TBT is thiophene-benzothiadiazole-thiophene). When the P3HT chain is linked to the TBT unit, we observe formation of a localized charge transfer state, with red-shifted absorption and emission. Independent of the excitation energy, this state is formed very rapidly (<40 fs) and efficiently. Because there is only a single TBT unit present, there is little scope for long-range charge separation and it is relatively short-lived, <1 ns. In contrast, when the P3HT chain and TBT unit are separated by the wider bandgap F8 unit, there is little indication for modification of either ground or excited electronic states, and longer-lived charge separated states are observed.

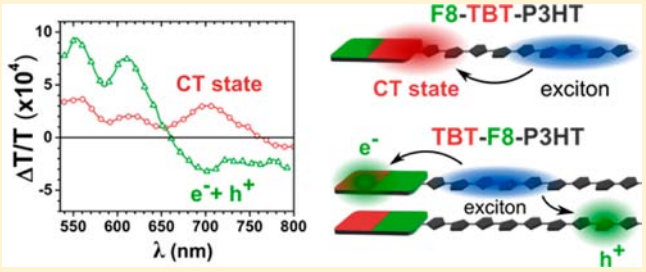

INTRODUCTION

Organic photovoltaics (OPV), in particular those that are solution processable, have the potential to provide low cost photovoltaic cells because they can be made flexible, robust, and lightweight using roll-to-roll processing. Currently, the highest power conversion efficiencies are obtained from low bandgap push−pull polymers blended with fullerene acceptors.[1] However, the strong optical absorption and tunable energy levels of push−pull polymers also make them candidates for electron acceptors in polymer:polymer photovoltaics.[2] The active structure of an OPV device is the heterojunction formed by the phase separation of two distinct organic materials, the donor and acceptor, which facilitates splitting of photo generated excitations. For polymeric organic materials the exciton diffusion length is small, typically 5−10 nm, so domains of the donor and acceptor must have one dimension of this order for efficient exciton migration to the donor/acceptor interface and so efficient generation of charge carriers.[3,4] However, to form spatially separated charges and avoid recombination, an electron and hole must separate to a distance at which their thermal energy is sufficient to overcome the Coulomb potential. In organic semiconductors, this distance, the geminate charge capture radius, is >15 nm so the film structure must be such that the charges have the opportunity to exceed this separation.[5,6] Additionally, the thickness of the active layer must be ∼100 nm to absorb sufficient light, and a percolating network of both donor and acceptor throughout this thickness is required for transport of charge carriers to the electrodes. These morphological requirements must be carefully balanced and highlight the importance of an ordered nanostructure. Most current organic photovoltaics depend upon demixing from a common solvent, to form nonequilibrium, interpenetrating donor/acceptor structures, which have been optimized empirically. However, block copolymers are known to self-assemble, through the restricted phase separation of the blocks, into thermodynamically stable, well-ordered nanostructures with relevant domain widths and lengths for photovoltaic devices.[7−13] Block copolymers can also act as polymeric surfactants in a

Received: December 17, 2012
Published: March 12, 2013

   dx.doi.org/10.1021/ja3121247 | J. Am. Chem. Soc. 2013, 135, 5074−5083

conventional blend structure to control the morphology, a process known as compatibilization.[14−17] Hence, block copolymers formed of active conjugated polymers are attractive candidates for all polymer solar cells. Although literature devices work through interchain charge separation between donor and acceptor units, the introduction of a conjugated intrachain linkage between donor and acceptor blocks offers an alternative route through intrachain charge separation.

As the coupling between the two blocks will form the heterojunction over which charge separation occurs, conjugated block copolymers will additionally allow for interfacial modification in terms of structure, crystallinity, and electronic properties. This extends the possibilities for achieving efficient charge separation at the interface in all polymer solar cells. It is therefore important to understand the photophysical and electronic behavior of the coupling between the sections of the block copolymer. Direct coupling with conjugation maintained between the blocks is currently of interest as it is expected that coupling in which conjugation is maintained throughout will be more favorable for charge separation than a nonfunctional linker as the distance across which charge separation must occur is reduced, the insulating linker is removed, and through-bond coupling would enhance the electron transfer rate. On the other hand, however, the charge recombination rate may also be expected to increase because electron and hole may remain in close proximity. Hence, investigation into the behavior of the conjugated coupling, especially the electronic properties, is of great interest. Because of challenges in the synthesis and purification, there are a limited number of studies, and the field of block copolymers with conjugation maintained throughout is still developing.[12,18−23] In this work, the parent system of study is P3HT (poly(3-hexylthiophene)) as the donor with F8TBT (poly[(9,9-dioctylfluorene)-2,7-diyl-*alt*-[4,7-bis(3-hexylthien-5-yl)-2,1,3-benzothiadiazole]-2,2-diyl]) as the acceptor, a conventional blend of which is one of the better performing all-polymer solar cells with a power conversion efficiency of 1.8%.[24] Similar all-polymer blends have achieved greater efficiencies up to 2.7%.[25] Using a closely related block copolymer of P3HT and PFTBTT (F8TBT without side chains on thiophene units and with branched side chains on F8 units) in a ternary blend, the morphology stabilizing role of this type of block copolymer was recently demonstrated.[21]

To understand the properties of the direct conjugated coupling in F8TBT-*b*-P3HT block copolymers, two model "end-functionalized" P3HT systems have been synthesized.[20,26,27] In these materials, a single electron-accepting F8TBT segment is added directly to the end of the donor P3HT chain, and they are novel in that the F8TBT unit can be connected through either the F8 or the TBT (Figure 1) with conjugation maintained throughout. These well-defined structures facilitate the study of the intramolecular interface in copolymers and provide insight into tuning this interface. In particular, these molecules allow us to investigate changes in intramolecular charge transfer (CT) states and charge separation when the nature of the conjugated coupling is altered by changing the point of linkage. The conclusions drawn from the study of these molecules are not material specific, and as well as aiding current understanding they can also guide the design of full diblock copolymers.

In this work, the photophysical properties of the direct conjugated coupling in the model end-functionalized P3HT-F8TBT systems were studied using time-resolved photoluminescence and transient absorption spectroscopy. It was found that the type of coupling is extremely important in determining the electronic properties of states at this intramolecular interface. Coupling through the F8 unit, with lower HOMO (highest occupied molecular orbital) and higher LUMO (lowest unoccupied molecular orbital) than both the donor and the acceptor, prevents electronic interaction of the donor and acceptor across the intramolecular interface and so maintains the original electronic properties of the photovoltaic blend. However, when coupling through the strongly electron accepting TBT moiety, the electronic properties of the states at the intramolecular interface are modified, resulting in the formation of intramolecular charge transfer states.

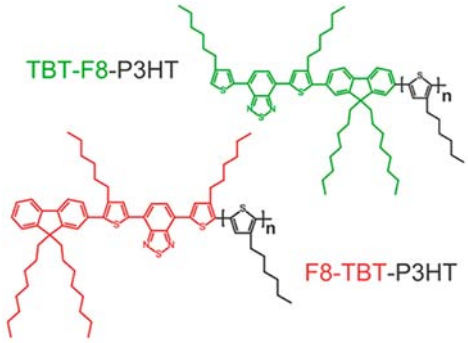

Figure 1. Chemical structures of end-functionalized P3HT molecules, n = 18.

EXPERIMENTAL DETAILS

Materials. The synthesis of the F8-TBT-P3HT, TBT-F8-P3HT, and P3HT materials proceeds via Kumada catalyst transfer polycondensation and is described in detail elsewhere.[20,26−28] The relevant properties of the materials are summarized in Table 1. The

Table 1. Physical Properties of Materials Studied

	P3HT	F8-TBT-P3HT	TBT-F8-P3HT
number of P3HT units [NMR]	24	18	18
M_n [NMR] (kg/mol)	4.0	3.85	3.85
M_n [GPC] (kg/mol)	6.6	6.0	5.7
functionalization [NMR] (%)		77	95
PDI [GPC]	1.12	1.07	1.07
contour length (nm)	9.5	9.1	9.1

number of P3HT units and the degree of functionalization were calculated from the ^{1}H NMR spectra. M_n was estimated using the number of P3HT units both from NMR and from GPC. Polydispersity indices (PDI) were taken from GPC. The contour length was obtained from the NMR degree of polymerization multiplied by the P3HT monomer repeat unit length, as measured by X-ray scattering. Details can be found in the aforementioned works and the Supporting Information. F8TBT was synthesized as described elsewhere.[20] Solutions were made in chlorobenzene (5 μg/mL) and prepared in a nitrogen atmosphere. Solutions were measured in quartz cuvettes (Hellma). Thin films of the materials were spin-coated at 1500 rpm for 60 s from 20 mg/mL 70 °C xylene (mixed isomers) solution. Quartz spectrosils, precleaned by consecutive sonication in acetone then isopropanol, were used as the substrate. The films were then annealed at 140 °C for 10 min followed by a fast quench cooling to achieve high P3HT crystallinity throughout the film and increase the likelihood of high polaron yield as seen in conventional P3HT + F8TBT blends.[29] All preparation was done in nitrogen atmosphere. The same preparation method was also used to make a 50:50 wt % blend of P3HT and F8TBT.

dx.doi.org/10.1021/ja3121247 | J. Am. Chem. Soc. 2013, 135, 5074−5083

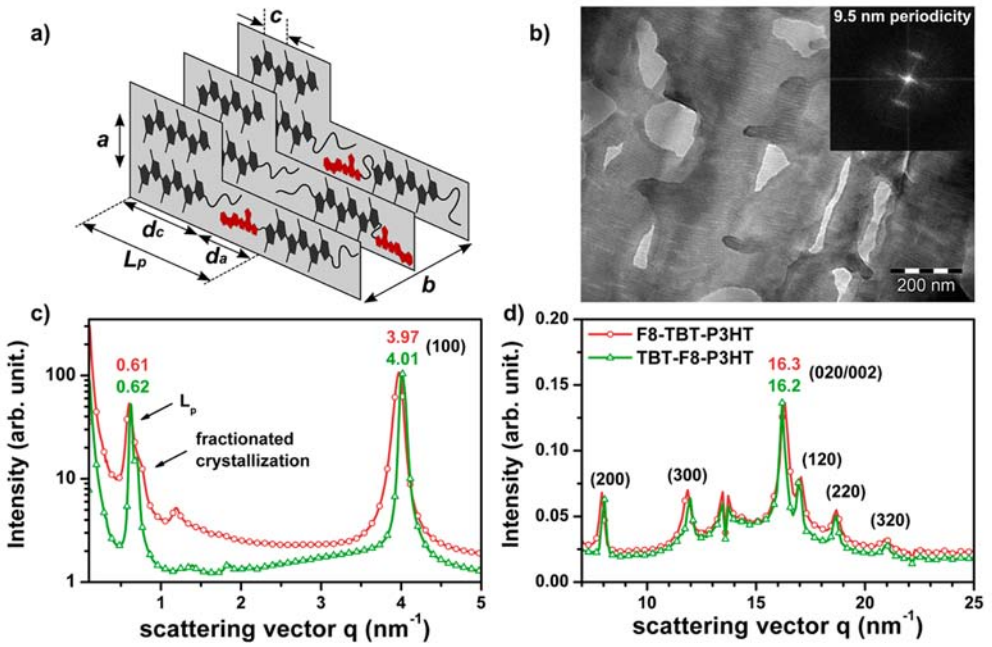

Figure 2. (a) Schematic of the chain extended crystal structure adopted by end-functionalized P3HT molecules. (b) TEM image of F8-TBT-P3HT thin film showing alternating crystalline and amorphous regions. Inset is the fast Fourier transform of the TEM image, which indicates 9.5 nm periodicity for the long period, L_p. (c) SAXS and (d) WAXS spectra used to determine lattice parameters of F8-TBT-P3HT and TBT-F8-P3HT. The long periods measured by SAXS are 10.3 and 10.1 nm, respectively.

X-ray Scattering. Combined small and wide-angle X-ray scattering (SAXS/WAXS) was carried out at the Diamond Light Source, UK, beamline I22. The samples were pressed as a polymer powder into small aluminum discs with an aperture of 0.8 mm and 1 mm in thickness, providing free-standing samples. Before the samples were measured at room temperature, the samples were heated above their melting temperature to 180 °C and cooled at a rate of 10 K/min in an inert gas atmosphere to obtain comparable thermodynamically equilibrated structures.

Transmission Electron Microscopy. Oriented films of F8-TBT-P3HT were prepared on clean glass substrates using slow-rate directional epitaxial crystallization following the protocol by Hartmann et al.[30] The highly oriented areas were identified for TEM analysis by optical microscopy (Leica DMR-X microscope). The films were coated with a thin amorphous carbon film, and the carbon-coated films were removed from the glass substrate by using poly(acrylic acid) (25% aqueous solution, Aldrich) and subsequently recovered onto TEM copper grids. TEM was performed in bright field, high resolution, and diffraction modes using a CM12 Philips microscope equipped with a MVIII (Soft Imaging System) CCD camera.

Steady-State and Time-Resolved Photoluminescence. Photoluminescence decay kinetics were measured by time-correlated single photon counting (TCSPC). The excitation source was a pulsed 470 nm, 80 ps full width at half-maximum, 10 MHz diode laser (PicoQuant LDH400), and the luminescence was detected using a microchannel plate photomultiplier (Hamamatsu Photonics) coupled to a monochromator and TCSPC electronics (Lifespec-ps and VTC900 PC card, Edinburgh Instruments). Time-resolved photoluminescence spectra can be constructed from decay kinetics measured over a range of wavelengths. With the same 470 nm laser excitation source, "steady-state" photoluminescence spectra were taken using a 500 mm spectrograph (SpectraPro2500i, Princeton Instruments) combined with a CCD camera (PIXIS 100-F, Princeton Instruments). UV−vis measurements were taken using a Hewlett-Packard 8453 spectrophotometer.

Photoluminescence Quantum Efficiency. Thin film photoluminescence quantum efficiencies (PLQE) were measured at room temperature in a nitrogen-purged integrating sphere with 501.7 nm excitation from an argon ion laser and detection with an Oriel Instaspec IV spectrometer. PLQE values were calculated as described by de Mello et al.[31] Solution PLQEs were estimated from comparison of the absorption and emission spectra to a fluorescent standard. Details are in the Supporting Information.

TA Spectroscopy. A Ti:sapphire amplifier system (Spectra-Physics, Solstice) was used to generate a train of 90 fs pulses at 1 kHz. Portions of the 800 nm output were used to pump a TOPAS optical parametric amplifier (Light Conversion) and a home-built broadband noncollinear optical parametric amplifier (NOPA). This allowed for probe light to be generated in the 540−800 nm and 825−1000 nm ranges, depending on the NOPA alignment. For measurements from 100 fs to 2 ns, the TOPAS was used as the pump beam, and the broadband probe from the NOPA was delayed using a mechanical stage (Newport). For measurements with 40 fs time resolution, a broadband (540−640 nm) pump pulse was used, compressed with a femtoJock (Biophotonic Solutions) employing the MIIPS method. For measurements from 1 ns to 1 ms, electronically delayed 600 ps fwhm excitation pulses were provided by a frequency-doubled Q-switched Nd:YVO4 laser (AOT-YVO-25QSPX, Advanced Optical Technologies). Every second pump pulse was blocked with a mechanical chopper for the 100 fs to 2 ns measurements and omitted electronically when using the Nd:YVO4 laser. The pump and probe beams were focused to the same spot on the sample, and then each probe pulse was detected and the differential transmission ($\Delta T/T$) calculated after averaging 1000 "pump on" and "pump off" shots for each data point. Prior to striking the sample, a portion of the probe beam was split off as a reference, passed through the sample, and used to correct for shot-to-shot variation in the probe. Both probe and reference beams enter a spectrograph (Princeton Instruments, Acton SpectraPro 2150i) offset vertically and are spectrally dispersed onto two 256-pixel photodiode arrays (Hamamatsu S3901256Q). Samples were measured under vacuum (10^{-5} mbar) during TA measurements at room temperature.

Quantum Chemical Calculations. Electronic states of the end-functionalized systems were characterized by semiempirical INDO Hamiltonian combined with an SCI scheme based on ground-state geometries optimized in the gas phase by DFT method using B3LYP functional with 6-31G** basis set.[32,33] The geometry comprises 20 repeat units of thiophene with a F8TBT monomer at the end. The

dx.doi.org/10.1021/ja3121247 | J. Am. Chem. Soc. 2013, 135, 5074−5083

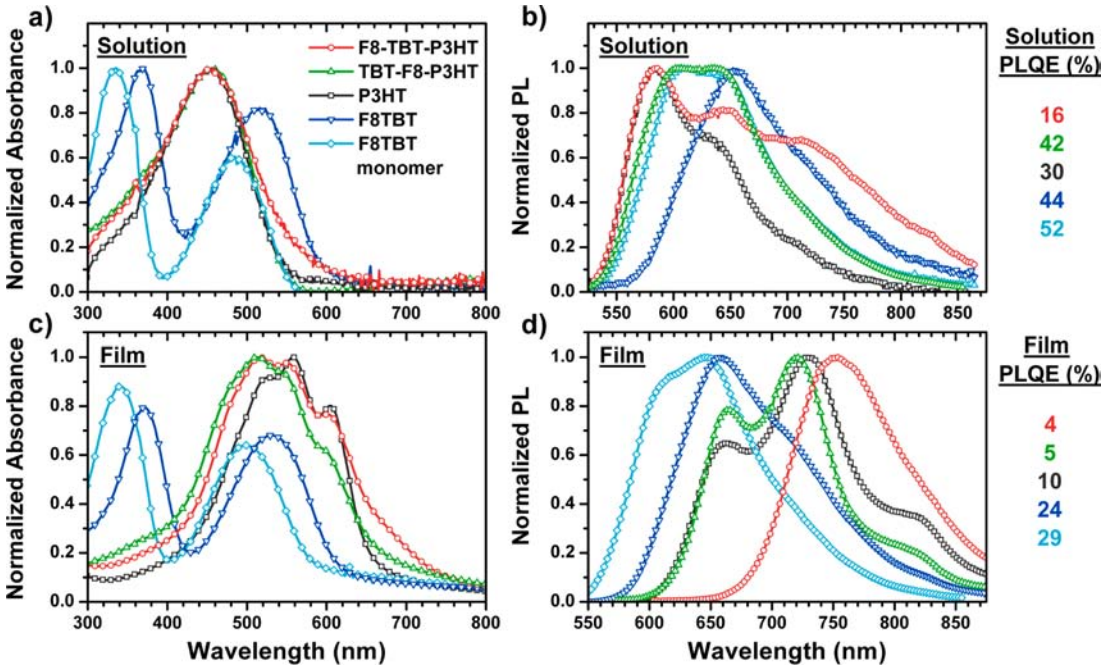

Figure 3. Steady-state absorption in (a) solution and (c) thin film, and photoluminescence spectra in (b) solution and (d) thin film, for the end-functionalized P3HT molecules and their parent materials. Excitation wavelength for PL spectra is 470 nm. The corresponding thin film and solution PLQE values are shown on the right.

hexyl chains were replaced by methyl groups in the geometry optimization to reduce computation time but still maintain conformational constraints induced by the side chains.

RESULTS AND DISCUSSION

Thin Film Structural Characterization. The semicrystalline morphology of the end-functionalized molecules is shown schematically in Figure 2a. Small angle (SAXS) and wide angle (WAXS) X-ray scattering, Figure 2c and d, respectively, show alternating crystalline and amorphous layers for both F8-TBT-P3HT and TBT-F8-P3HT. These form superstructures with periodicity $L_P = d_c + d_a$ of 10.3 and 10.1 nm, respectively, where L_P is the long period. This occurs in particular for P3HT of lower molecular weight and low polydispersity.[34] Within the lamellar crystal layers, the thiophene backbones π-stack along the *b*-axis, and along the *a*-axis the main chains are separated by "sheets" of the alkyl chains. The positions of the (100) and the (020)/(002) reflections in Figure 2c and d indicate that these lattice parameters are similar to those of pure P3HT in literature.[28] The alternating crystalline and narrow amorphous regions are particularly well observed in highly oriented thin films of F8-TBT-P3HT, grown by directional epitaxial crystallization,[35] using transmission electron microscopy (TEM) in the bright-field mode. Figure 2b shows a representative bright field image of a highly oriented F8-TBT-P3HT film. The inset in Figure 2b is the fast Fourier transform of the TEM image. It shows two broad reflections corresponding to the first order of the lamellar structure with a total periodicity (crystalline plus amorphous zones) of 9.5 nm, in good agreement with the X-ray data. The ~9.1 nm average contour length of the F8-TBT-P3HT chain, taken as the length of a single thiophene (0.39 nm from 002 peak in WAXS spectrum) multiplied by the number of thiophene units (see Table 1), plus the F8TBT unit length (2.0 nm), is very similar to the long period from which we can conclude that fully chain extended crystals are formed. The X-ray scattering data show that with the addition of the single F8-TBT unit the P3HT order is preserved and confirms that chain extended crystals are formed. This is also evident from the absorption and emission spectra shown in the following section. The F8-TBT end group must therefore reside in the amorphous regions between the crystalline lamellae as depicted in Figure 2a. This is further supported by the electron diffraction pattern of the oriented films grown by directional epitaxial crystallization (see Supporting Information Figure S1). The obtained diffraction pattern is characteristic of a $[01\bar{1}]$ zone and is identical to that obtained for a highly orientated P3HT sample; that is, it shows the form I structure identified by Kayunkid et al.[36] Accordingly, so as not to perturb the crystalline packing of P3HT segments, F8-TBT end groups must be rejected to the narrow amorphous interlamellar zones. We note that the accommodation of the F8TBT units within the amorphous regions is similar to the take up of the fullerene acceptor PCBM in low weight fraction P3HT:PCBM blends.[37]

Steady-State Absorption and Emission. Figure 3 shows the steady-state absorption and photoluminescence (PL) spectra of the end-functionalized P3HT molecules and their constituent parent materials, both in thin film and a chlorobenzene solution. The first striking difference to be noted is the change in the absorption and PL of P3HT upon moving from solution to thin film. This is due to the formation of weakly interacting H-aggregates in thin film, as described in the literature,[38] which results in a significantly red-shifted, well-defined, vibronic structure with a reduced 0−0 peak intensity in emission. For F8-TBT-P3HT, in both solution and thin film, the presence of a PL emission signal, further red-shifted (λ_{max} = 725 nm in solution, λ_{max} = 750 nm in thin film) as compared to the pure parent materials, and a new, weak subgap absorption band, is indicative of the formation of a charge transfer state.[39−41] The measurements in dilute solution, Figure 3b, confirm that this is an intramolecular state and is present in the absence of aggregation. To clarify, it is well-known that the

dx.doi.org/10.1021/ja3121247 | J. Am. Chem. Soc. 2013, 135, 5074−5083

lowest energy excitons in push−pull type polymers, such as F8TBT, have significant charge transfer character,[42] but from here on "CT state" will refer to the newly observed intramolecular state in the F8-TBT-P3HT molecule unless stated otherwise. It is important to note that with excitation deep in the P3HT band ($\lambda_{ex} \approx 470$ nm), only a fraction of the photogenerated excitons can migrate to the lower energy CT state when the chains exhibit a high degree of torsional disorder in solution, hence the significant P3HT emission (16% total PLQE, 10% from P3HT + 6% from CT state). From the time-resolved emission spectra (see Figure 4c), the distinct

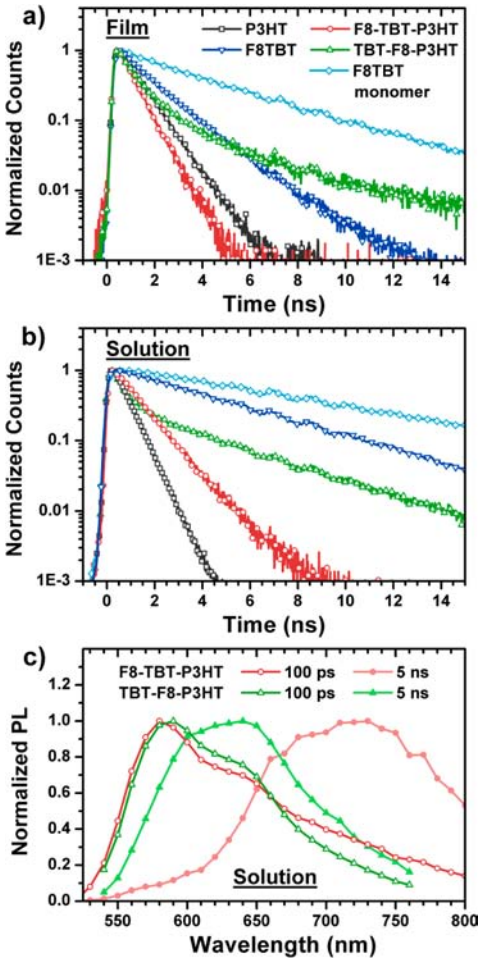

Figure 4. Photoluminescence decay of end-functionalized P3HTs and constituent materials measured by TCSPC in (a) thin film and (b) solution. Excitation wavelength is 470 nm, and detection is at peak emission wavelengths shown in Figure 3 except in the case of F8-TBT-P3HT in solution for which it is 750 nm (to avoid the decay of residual P3HT component). (c) Time-resolved spectra of the end-functionalized molecules at 100 ps and 5 ns constructed from TCSPC measurements.

contributions from P3HT excitons and the CT state can clearly be seen. In contrast, the planarized, less disordered P3HT aggregates in the thin film promote very efficient transfer of the photogenerated excitons to the CT state, resulting in a complete quenching of P3HT emission and so photoluminescence solely from the CT state. The strong absorption and fast emission indicate a relatively high oscillator strength, in contrast to the very low level of coupling in intermolecular charge transfer states observed in conventional photovoltaic blends[43] (this can also be seen when comparing the absorption and PL of the F8-TBT-P3HT to a conventional blend of F8TBT + P3HT; see Supporting Information Figure S2). The lack of these absorption and emission features in the TBT-F8-P3HT material shows that no intramolecular charge transfer state with significant oscillator strength is formed. In solution, the lowest energy state is localized on the TBT-F8, energy transfer to this occurs, and the PL resembles that of the F8TBT monomer with some residual P3HT emission. The high PLQE of the TBT-F8-P3HT molecule in solution indicates that there is little (<10%) intrachain charge transfer. A detailed analysis is included in the Supporting Information. In thin films, the P3HT H-aggregate states are the lowest energy neutral states, and emission is therefore predominantly from P3HT. However, from the PLQE data, it is significantly quenched as compared to both P3HT and F8TBT. As we report below, transient absorption reveals the formation of charge-separated states; we consider these arise from interchain processes similar to the charge transfer states formed in conventional polymer:polymer photovoltaic blends.

Fluorescence Lifetime. The decay lifetimes of the emissive species were measured, in both solution and thin film, using time correlated single photon counting (TCSPC) and are shown in Figure 4 for excitation at 470 nm. Detection in each case is at the peak wavelength shown in Figure 3 except for F8-TBT-P3HT in solution where the decay shown is for 750 nm to measure the decay of the CT state rather than the residual P3HT excitons, which cannot reach the CT state at the end of the molecule. Figure 4c shows time-resolved emission spectra for the end-functionalized molecules in solution, constructed from TCSPC measurements made at a range of detection wavelengths. Because of their increased electron−hole separation, charge transfer states typically have longer lifetimes than singlet excitons in the individual homopolymers.[44] This can clearly be seen in solution for F8-TBT-P3HT versus P3HT as expected. However, in thin film, P3HT forms weakly interacting H-aggregates, which increases the lifetime of P3HT excitons in contrast to amorphous polymers, for example, F8TBT, in which the PL lifetime decreases upon going from solution to thin film. This explains the apparently shorter lifetime of the charge transfer state in F8-TBT-P3HT as compared to P3HT in thin film. Note that the decay dynamics are independent of detection wavelength for P3HT and F8-TBT-P3HT in thin film. For TBT-F8-P3HT in solution, energy transfer to the lowest energy state localized on the TBT-F8, followed by emission from this state, is observed with a fraction of residual P3HT emission. In thin films, emission is predominantly from P3HT. The long-lived component, with spectral shape of P3HT and dispersive decay kinetics, is considered to arise from repopulation of the P3HT singlet by the recombination of charge separated states. The mono-exponential decay in solution for times >3 ns further suggests that charge separation predominantly proceeds interchain and is minimal in solution.

Transient Absorption. To verify the picture suggested by the steady-state and time-resolved photoluminescence, and elucidate details of this model, transient absorption measurements were performed on thin films. Transient absorption spectroscopy is the measurement of the differential transmission ($\Delta T/T$) of a sample, and its temporal evolution, after a pump pulse generates new photoexcited species. Additional transmission (positive $\Delta T/T$) can be caused by depopulation of the ground state, termed ground-state bleach (GSB), or can

dx.doi.org/10.1021/ja3121247 | J. Am. Chem. Soc. 2013, 135, 5074−5083

arise from stimulated emission (SE) of photoexcited species. Reduced transmission (negative $\Delta T/T$) is photoinduced absorption (PIA) due to the excited-state species present. The evolution of these signals over time allows the population dynamics of photoexcited species to be probed. Figure 5a shows typical transient absorption spectra of a thin film of P3HT, the parent molecule of the end-functionalized materials. The ground-state bleach has characteristic peaks at 560 and 610 nm, while the stimulated emission peaks at 725 nm. On time scales >2 ns, the majority of the singlet excitons have decayed and few excited species remain (no PIA observed). The positive signal remaining arises from a thermal artifact.[45] Focusing on F8-TBT-P3HT, it is interesting to note the unusual features of the transient absorption spectra, presented in Figure 5b. The ground-state bleach does not, as might be expected, resemble the steady-state absorption spectrum but rather shows a feature peaking at 700 nm, of magnitude similar to that of the expected P3HT GSB peaks at 560 and 610 nm. This is observed independent of the excitation wavelength (see Supporting Information Figure S3). Upon consideration of the spectral location, between the P3HT GSB and CT state PL, and the lifetime, similar to the PL lifetime of the CT state but with a fraction persisting to microsecond time scales, we assign this to the ground-state bleach of the intramolecular charge transfer state. A direct spectral comparison is shown in Supporting Information Figure S4, and, again, a similar feature is also seen in the TA spectrum of a dilute solution (Supporting Information Figure S5). The kinetics of the PIA in the near-infrared range is well correlated with this CT GSB feature and is assigned to its PIA. The most plausible explanation for this relative enhancement of the GSB of the CT state is transfer, or localization, of the initially excited state to the CT state at the end of the molecule as after this has taken place the GSB would preferentially result from the red-shifted CT state absorption. Figure 5c shows the kinetics of the CT GSB, averaged over the 680−720 nm range, with the PL decay of the CT state included for comparison. The −100 to 100 fs data were measured using the broadband (540−640 nm) pump setup, and the blue line in Figure 5c is a fit corresponding to an instrument response (fwhm) of 40 fs. (See Supporting Information Figure S6 for details.) This implies the intramolecular CT state is populated within the 40 fs time resolution. As no other explanation can account for the relative enhancement of the GSB of the CT state at such early times, this leads us to conclude that localization of the initially excited state to the CT state occurs within 40 fs. It is also noted that for the same excitation density (correction has been made for relative absorption of samples at the excitation wavelength), the magnitude of the GSB in F8-TBT-P3HT is significantly smaller, by approximately a factor of 4, than the GSB of P3HT. This is consistent with ultrafast localization to the CT state in the end-functionalized molecule as the absorption of the CT state is weak as compared to that of P3HT as shown in Figure 3, and localization to the CT state at the end of the chain would leave much of the chain unbleached. Combined with the fact that in the thin film of F8-TBT-P3HT no PL from P3HT singlet excitons is observed, see Figure 3, the TA spectra suggest that the initially created photoexcitations are localized on the CT state at the end of the F8-TBT-P3HT molecules with an efficiency approaching 100%. This is interesting considering 23% of the molecules are not functionalized and implies a strong driving force for localization to the CT state, the mechanism of which must take into account an interchain component for some of the excitations. From the plot of the CT state kinetics in Figure 5c, it can be seen that approximately 90% of the CT states decay to the ground state exponentially with the lifetime of 660 ps that describes the photoluminescence. The remaining ∼10% of the signal persists to later times and, to a basic approximation, decays according to a power law with exponent −0.3. We consider that this is due to some fraction of the F8-TBT-P3HT CT states dissociating further, with one charge remaining on the functionalized end of the molecule, so bleaching the CT state (most likely the electron localized on the BT unit) and the other somewhere in the P3HT crystalline domain. This is supported by the similar decay kinetics of charge pairs formed in a conventional P3HT/F8TBT blend; see Supporting Information Figure S7. No evidence of triplet formation is observed, most likely because there will still be a significant exchange energy for the CT state due to the close proximity of electron and hole density, that is, the excitonic nature of this CT state, so intersystem crossing is just too slow. The relatively short CT state lifetime and small likelihood of dissociation is not beneficial for potential photovoltaic materials but may be

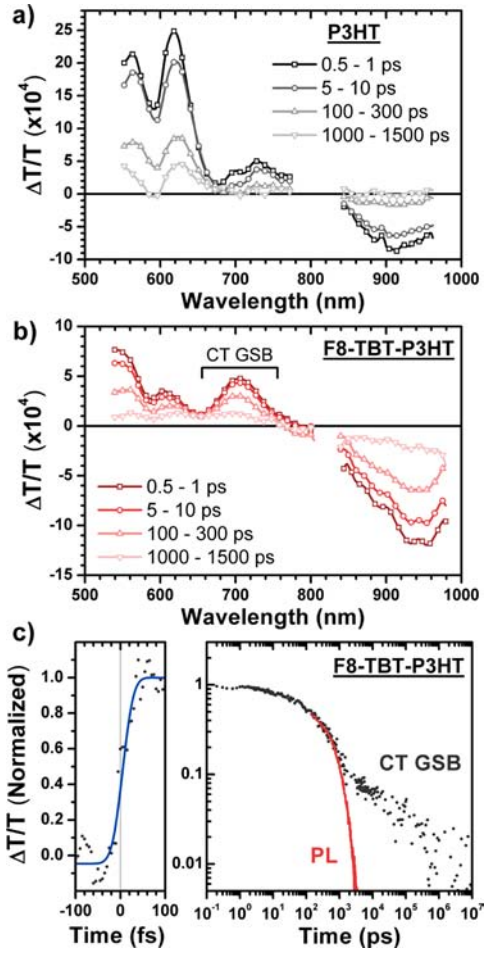

Figure 5. Thin film transient absorption spectra of (a) P3HT and (b) F8-TBT-P3HT, highlighting the enhanced ground-state bleach of the CT state (λ_{ex} = 500 nm, 6 μJ cm^{-2} per pulse). The normalized decay kinetics of the CT state GSB (c) are also shown, averaged over the 680−720 nm range, with the PL decay of the CT state (exponential decay with lifetime 660 ps) included for comparison. The −100 to 100 fs data were measured using a setup with 40 fs resolution. The >2 ns kinetics were measured with λ_{ex} = 532 nm, 15 μJ cm^{-2} per pulse (scaled to match <2 ns data).

dx.doi.org/10.1021/ja3121247 | J. Am. Chem. Soc. 2013, 135, 5074−5083

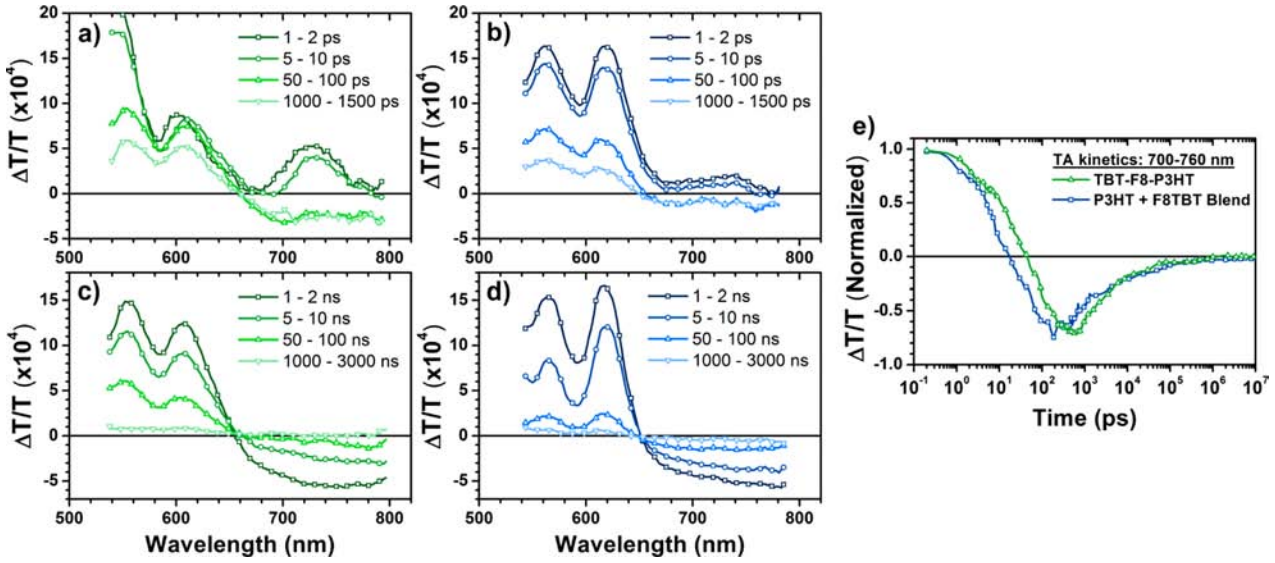

Figure 6. Thin film transient absorption spectra of TBT-F8-P3HT on (a) picosecond and (c) nanosecond time scales as compared to a P3HT and F8TBT blend on (b) picosecond and (d) nanosecond time scales. Excitation wavelength is 500 nm (6 μJ cm^{-2} per pulse) and 532 nm (15 μJ cm^{-2} per pulse) for picosecond and nanosecond TA, respectively. Part (e) shows the temporal evolution of the TA signal averaged over 700−760 nm.

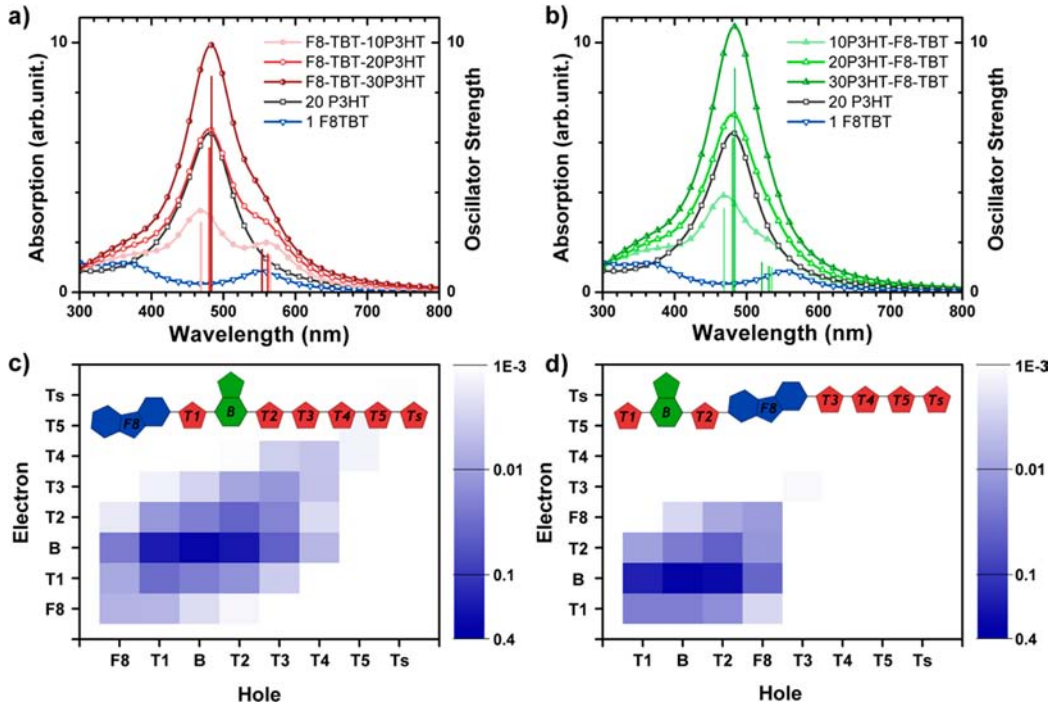

Figure 7. Calculated ground-state absorption spectra of (a) F8-TBT-P3HT in which the hole density is partly delocalized along the P3HT chain in the first excited state and (b) TBT-F8-P3HT in which the F8 units prevent delocalization of the first excited-state wave function along the P3HT chain. The bars indicate the first and second excited states and corresponding oscillator strength. The calculations are shown for P3HT lengths of 10, 20, and 30 units. Parts (c) and (d) show the probability (indicated by the log-scale color bars) of finding the hole in the π-orbital on the x-axis site and the electron in the π-orbital on the y-axis site for the first excited states of F8-TBT-P3HT and TBT-F8-P3HT, respectively. The sites are the structural units shown in the insets.

expected in this molecule as there is no energetically or spatially favorable route for the electron to follow, so it remains localized at the BT unit, bound in the CT state, which cannot further dissociate to separated charge carriers. In a practical block copolymer system, the additional extent of the acceptor block, and other chains in the acceptor domain, would be available for the electron so it is hoped dissociation could proceed. However, it may be that direct conjugated linkage of the donor and acceptor will be detrimental to photovoltaic performance if a strongly bound, intramolecular CT state with large oscillator strength is formed, which acts as a trap and facilitates recombination to the ground state.

The thin film transient absorption spectra of TBT-F8-P3HT, presented in Figure 6a and c, differ significantly from the variant conjugated through the TBT. After excitation the typical features of P3HT are seen: GSB peaks at 560, 610 nm and SE

dx.doi.org/10.1021/ja3121247 | J. Am. Chem. Soc. 2013, 135, 5074−5083

peaking at approximately 725 nm, with no evidence of any large oscillator strength intramolecular CT state. The stimulated emission signal decays with a lifetime of approximately 50 ps, see Figure 6e, and the spectra evolve to show a broad, flat PIA extending out into the infrared, a signature of separated charge carriers. This is very similar to the transient absorption spectra of a conventional blend of P3HT and F8TBT (50:50 wt %) as shown in Figure 6b and d and observed in the literature.[2] The difference in the P3HT GSB region at times <50 ps reflects the differences in steady-state absorption spectra caused by the lower P3HT crystallinity in the TBT-F8-P3HT. At longer times, these more amorphous, higher energy sites are no longer populated. These data indicate that conjugation through the F8 unit prevents electronic intermixing of the P3HT donor and BT acceptor orbitals across the intramolecular interface and so, in general, maintains the original electronic properties of the photovoltaic blend. We consider that this is due to the bridging F8 unit with a wider bandgap having a lower HOMO and higher LUMO (−5.7 and −0.8 eV, respectively) than both the P3HT donor (HOMO, −4.4 eV; LUMO, −2.2 eV) and the TBT acceptor (HOMO, −5.3 eV; LUMO, −2.6 eV). HOMO and LUMO values are obtained from DFT B3LYP calculations, with a 6-31G* basis set, on a single F8 unit, a chain of 16 P3HT units, and a single TBT unit, respectively.[32] This is consistent with previous studies,[46] one of which shows that insertion of F8 between BT units decreases the coupling between the BT units and so decreases the electron mobility along the chain.[47] It is not clear whether the charge photogeneration seen in this system results from an intrachain process across this weak coupling or from interchain charge transfer. However, the solution PLQE (Figure 3b and Supporting Information) and solution TA data (Supporting Information Figure S8) suggest the fraction of intrachain charge separation is low. The similar magnitudes of the PIA signals (Figure 6e) for both the P3HT:F8TBT blend and the TBT-F8-P3HT, despite the blend being 50% by weight F8TBT while the TBT-F8-P3HT is effectively ∼20% F8TBT, indicates that the generation of charge in TBT-F8-P3HT is as effective as the standard blend and is not hampered by the conjugated linkage. Also, the conjugated linkage does not provide a more efficient pathway for charge recombination as there is no significant increase in the charge recombination rate.

Quantum Chemical Calculations. To further explore the nature of the intramolecular charge transfer state in F8-TBT-P3HT, and its absence in TBT-F8-P3HT, quantum chemical modeling of the molecules was performed as described in the Experimental Details. This was done using an active space of 60 occupied and 60 unoccupied molecular orbitals in the gas phase so is most closely comparable to the experimental results in solution. The LUMO is localized on the TBT unit, whereas the HOMO is delocalized across the whole molecule, with large weights on the P3HT chain, as seen in related polymers[48] (see Supporting Information Figure S9 for HOMO and LUMO topologies). The calculated F8-TBT-P3HT absorption spectra in Figure 7a reveal the presence of the red shoulder, consistent with the experimental observation. This red shoulder absorption was assigned to the lowest excited state with CT character, involving mainly the electronic transition from the P3HT donor (in particular the thiophenes near the BT unit) to the BT acceptor unit. We have also analyzed the characteristics of the electron−hole pairs in the lowest excited state. From the semiempirical calculations of this electronic state, we generate a two-dimensional grid where each point, (x,y), represents the probability, $|\psi(x,y)|^2$, of finding the hole in the π-orbital on site x and the electron in the π-orbital on site y. This is shown for F8-TBT-P3HT in Figure 7c, and in this case the sites are the structural units shown in the inset. The darkest regions refer to the highest probabilities according to the colorbar scale. For further details on the methodology, see the Supporting Information and Cornil et al.[46] The lowest excited state of F8-TBT-P3HT, Figure 7c, shows large contributions from charge transfer localized on the TBT unit and also confirms further intramolecular charge transfer at the interface of F8TBT and P3HT, with electrons on the benzothiadiazole unit of TBT and holes on the P3HT. This intramolecular charge transfer is not only localized at the interface of F8TBT and P3HT, but is also delocalized over more thiophene rings of the P3HT; for example, there is still a probability of 0.01 for finding electrons on the benzothiadiazole unit and holes on the second thiophene ring of P3HT away from the interface, labeled T4 in Figure 7c. However, this is not the case in the TBT-F8-P3HT molecule as the F8 prevents electronic interaction of the BT and thiophene rings in the TBT unit with those of P3HT. The absorption spectrum calculated for TBT-F8-P3HT with 20 P3HT units, shown in Figure 7b, does not show a significant red shoulder, and, as demonstrated in Figure 7d, the first excited state of TBT-F8-P3HT is only attributed to states localized on the F8TBT unit. This is consistent with the experimentally observed solution photoluminescence resembling that of the F8TBT monomer.

■ CONCLUSIONS

The advantage of our simple model system is that the single F8TBT acceptor segment does not interfere with crystallization of the P3HT block. This results in a well-controlled bulk structure with a clearly defined crystallized donor phase and the acceptor groups repelled into the amorphous regions between crystallites. This has enabled us to get the clear differentiation of operation for the two coupling regimes (through F8 and TBT, respectively) and draw solid conclusions concerning their behavior.

In a model system mimicking the intramolecular interface in a diblock copolymer, we have demonstrated that direct conjugated coupling of a strong donor block and a strong acceptor moiety, as in F8-TBT-P3HT, greatly modifies the electronic properties at the intramolecular interface. In F8-TBT-P3HT, there is electronic intermixing of the P3HT donor and BT acceptor, and a strong intramolecular CT state is formed at the coupling between the donor and acceptor as shown schematically in Figure 8a. In thin film, localization to this CT state is extremely fast (<40 fs) and occurs with efficiency approaching 100%. However, while the initial step of exciton localization to the CT state is very efficient and the electron and hole are somewhat separated, it is found that for this molecule the CT state itself has only a small probability of further dissociating, most likely as there is no energetically or spatially favorable path for the electron to diffuse away from the hole. Hence, 90% of the CT states formed decay radiatively on a time scale of 660 ps and do not form separated charge carriers. This is an example of a conjugated coupling that influences the electronic properties of the interface and, in principle, could be tuned to improve the efficiency of charge generation. Ideally a CT state would be formed, which acts as a precursor to the generation of free charge carriers, either via the delocalized nature of the CT state or through the formation of a cascading energy landscape, and so would increase the

dx.doi.org/10.1021/ja3121247 | J. Am. Chem. Soc. 2013, 135, 5074−5083

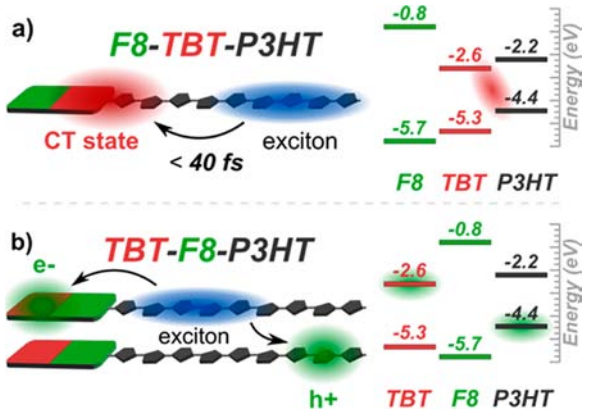

Figure 8. Schematic diagram of the dominant processes and relative energy levels in the model copolymers with different conjugated coupling. (a) F8-TBT-P3HT and (b) TBT-F8-P3HT.

efficiency of charge generation. However, it may be that direct conjugated linkage of a strong donor and acceptor will be detrimental to photovoltaic performance if a strongly bound, intramolecular CT state with large oscillator strength is formed, which acts as a trap and facilitates recombination to the ground state.

In contrast, coupling through a unit with lower HOMO and higher LUMO than both the donor and the acceptor prevents electronic interaction of the donor and acceptor across the intramolecular interface and so maintains the original electronic properties of the photovoltaic blend. Thus, for TBT-F8-P3HT, conjugation through the F8 prevents electronic intermixing of the P3HT donor and the BT acceptor, and the material exhibits independent P3HT and F8TBT behavior. In thin film, it can be observed that the exciton is not as efficiently drawn to the intramolecular interface as compared to F8-TBT-P3HT and a strong intramolecular CT state is not formed. However, when excitons reach an interface (inter- or intramolecular), they can be successfully split to form separated charge carriers as in conventional P3HT + F8TBT blends and with similar efficiency. Figure 8b shows this schematically. This is an example of a conjugated coupling that does not affect the electronic properties of the interface while also ensuring the close proximity of donor and acceptor. Block copolymers containing this type of bridging could be used to influence only the morphology of a photovoltaic device.

Therefore, for this particular material combination, direct conjugated coupling of the P3HT donor and strong TBT acceptor will be detrimental to photovoltaic performance as a strongly bound, intramolecular CT state is formed, which acts as a trap and facilitates recombination to the ground state. Coupling through the F8 results in long-lived charge carriers with a yield similar to conventional P3HT + F8TBT blends and so will give better photovoltaic performance.

In summary, the model system provides significant insight into the fundamental working of charge generation and separation at the intramolecular "interface" in copolymers. This work also highlights how the conjugated coupling in full diblock copolymers will significantly influence the interfacial electronic properties and that careful design is crucial if efficient photovoltaic cells are to be made.

■ ASSOCIATED CONTENT

Supporting Information

Additional details including solution photoluminescence quantum efficiency, contour length of F8-TBT-P3HT from X-ray scattering and NMR, electron diffraction pattern of F8-TBT-P3HT film grown by directional epitaxial crystallization, thin film absorption and PL including P3HT + F8TBT blend, F8-TBT-P3HT transient absorption, 700 nm excitation, F8-TBT-P3HT transient absorption, steady-state absorption and PL comparison, F8-TBT-P3HT versus P3HT transient absorption in solution, experimental details for TA measurements with 40 fs resolution, F8-TBT-P3HT CT state versus P3HT+F8TBT blend PIA: TA decay kinetics, TBT-F8-P3HT transient absorption in solution, and electronic structure calculations of end-functionalized molecules at semiempirical and ab initio levels of theory. This material is available free of charge via the Internet at http://pubs.acs.org.

■ AUTHOR INFORMATION

Corresponding Author

rhf10@cam.ac.uk

Present Address

[#]Institute of Macromolecular Chemistry, University of Freiburg, Stefan-Meier-Strasse 31, 79104 Freiburg, Germany.

Notes

The authors declare no competing financial interest.

■ ACKNOWLEDGMENTS

We thank Dr. Sergei Tretiak for helpful discussions. We thank the EPSRC (UK) and the ITN-SUPERIOR (PITN-GA-2009 − 238177) for financial support. D.B. is a FNRS research Director.

■ REFERENCES

(1) He, Z.; Zhong, C.; Su, S.; Xu, M.; Wu, H.; Cao, Y. *Nat. Photonics* **2012**, *6*, 593−597.
(2) Hodgkiss, J. M.; Campbell, A. R.; Marsh, R. A.; Rao, A.; Albert-Seifried, S.; Friend, R. H. *Phys. Rev. Lett.* **2010**, *104*, 1−4.
(3) Markov, D. E.; Amsterdam, E.; Blom, P. W. M.; Sieval, A. B.; Hummelen, J. C. *J. Phys. Chem. A* **2005**, *109*, 5266−74.
(4) Shaw, P. E.; Ruseckas, A.; Samuel, I. D. W. *Adv. Mater.* **2008**, *20*, 3516−3520.
(5) Groves, C.; Marsh, R. A.; Greenham, N. C. *J. Chem. Phys.* **2008**, *129*, 114903.
(6) He, X.; Gao, F.; Tu, G.; Hasko, D.; Hüttner, S.; Steiner, U.; Greenham, N. C.; Friend, R. H.; Huck, W. T. S. *Nano Lett.* **2010**, *10*, 1302−7.
(7) Fasolka, M. J.; Mayes, A. M. *Annu. Rev. Mater. Res.* **2001**, *31*, 323−355.
(8) Darling, S. B. *Energy Environ. Sci.* **2009**, *2*, 1266.
(9) Segalman, R. A.; McCulloch, B.; Kirmayer, S.; Urban, J. J. *Macromolecules* **2009**, *42*, 9205−9216.
(10) Sommer, M.; Huettner, S.; Thelakkat, M. *J. Mater. Chem.* **2010**, *20*, 10788.
(11) Scherf, U.; Gutacker, A.; Koenen, N. *Acc. Chem. Res.* **2008**, *41*, 1086−97.
(12) Verduzco, R.; Botiz, I.; Pickel, D. L.; Kilbey, S. M.; Hong, K.; Dimasi, E.; Darling, S. B. *Macromolecules* **2011**, *44*, 530−539.
(13) Barrau, S.; Heiser, T.; Richard, F.; Brochon, C.; Ngov, C.; Van de Wetering, K.; Hadziioannou, G.; Anokhin, D. V.; Ivanov, D. A. *Macromolecules* **2008**, *41*, 2701−2710.
(14) Yang, C.; Lee, J. K.; Heeger, A. J.; Wudl, F. *J. Mater. Chem.* **2009**, *19*, 5416.
(15) Sivula, K.; Ball, Z. T.; Watanabe, N.; Fréchet, J. M. J. *Adv. Mater.* **2006**, *18*, 206−210.

(16) Lee, J. U.; Jung, J. W.; Emrick, T.; Russell, T. P.; Jo, W. H. *J. Mater. Chem.* **2010**, *20*, 3287.
(17) Slota, J. E.; Elmalem, E.; Tu, G.; Watts, B.; Fang, J.; Oberhumer, P. M.; Friend, R. H.; Huck, W. T. S. *Macromolecules* **2012**, *45*, 1468−1475.
(18) Woody, K. B.; Leever, B. J.; Durstock, M. F.; Collard, D. M. *Macromolecules* **2011**, *44*, 4690−4698.
(19) Izuhara, D.; Swager, T. M. *Macromolecules* **2011**, *44*, 2678−2684.
(20) Sommer, M.; Komber, H.; Huettner, S.; Mulherin, R.; Kohn, P.; Greenham, N. C.; Huck, W. T. S. *Macromolecules* **2012**, *45*, 4142−4151.
(21) Mulherin, R. C.; Jung, S.; Huettner, S.; Johnson, K.; Kohn, P.; Sommer, M.; Allard, S.; Scherf, U.; Greenham, N. C. *Nano Lett.* **2011**, *11*, 4846−51.
(22) Tu, G.; Li, H.; Forster, M.; Heiderhoff, R.; Balk, L. J.; Scherf, U. *Macromolecules* **2006**, *39*, 4327−4331.
(23) Botiz, I.; Schaller, R. D.; Verduzco, R.; Darling, S. B. *J. Phys. Chem. C* **2011**, *115*, 9260−9266.
(24) McNeill, C. R.; Abrusci, A.; Zaumseil, J.; Wilson, R.; McKiernan, M. J.; Burroughes, J. H.; Halls, J. J. M.; Greenham, N. C.; Friend, R. H.; M, J. J. *Appl. Phys. Lett.* **2007**, *90*, 193506.
(25) Mori, D.; Benten, H.; Ohkita, H.; Ito, S.; Miyake, K. *ACS Appl. Mater. Interfaces* **2012**, *4*, 3325−3329.
(26) Komber, H.; Senkovskyy, V.; Tkachov, R.; Johnson, K.; Kiriy, A.; Huck, W. T. S.; Sommer, M. *Macromolecules* **2011**, *44*, 9164−9172.
(27) Senkovskyy, V.; Sommer, M.; Tkachov, R.; Komber, H.; Huck, W. T. S.; Kiriy, A. *Macromolecules* **2010**, *43*, 10157−10161.
(28) Kohn, P.; Huettner, S.; Komber, H.; Senkovskyy, V.; Tkachov, R.; Kiriy, A.; Friend, R. H.; Steiner, U.; Huck, W. T. S.; Sommer, J.-U.; Sommer, M. *J. Am. Chem. Soc.* **2012**, *134*, 4790−805.
(29) McNeill, C. R.; Halls, J. J. M.; Wilson, R.; Whiting, G. L.; Berkebile, S.; Ramsey, M. G.; Friend, R. H.; Greenham, N. C. *Adv. Funct. Mater.* **2008**, *18*, 2309−2321.
(30) Hartmann, L.; Tremel, K.; Uttiya, S.; Crossland, E.; Ludwigs, S.; Kayunkid, N.; Vergnat, C.; Brinkmann, M. *Adv. Funct. Mater.* **2011**, *21*, 4047−4057.
(31) De Mello, J. C.; Wittmann, H. F.; Friend, R. H. *Adv. Mater.* **1997**, *9*, 230−232.
(32) Frisch, M. J.; Trucks, G. W.; Schlegel, H. B.; Robb, M. A.; Cheeseman, J. R.; Scalmani, G.; Barone, V.; Petersson, G. A.; Nakatsuji, H.; Caricato, M.; Li, X.; Izmaylov, A. F.; Bloino, J.; Zheng, G.; Sonnenberg, J. L.; Ehara, M.; Toyota, K.; Fukuda, R.; Hasegawa, J.; Ishida, M.; Honda, Y.; Kitao, O.; Nakai, H.; Vreven, T.; Montgomery, J. A., Jr.; Peralta, J. E.; Ogliaro, F.; Bearpark, M.; Heyd, J. J.; Kudin, K. N.; Staroverov, V. N.; Keith, T.; Kobayashi, R.; Raghavachari, K.; Rendell, A.; Burant, J. C.; Iyengar, S. S.; Cossi, M.; Rega, N.; Millam, J. M.; Klene, M.; Knox, J. E.; Bakken, V.; Adamo, C.; Jaramillo, J.; Gomperts, R.; Yazyev, O.; Austin, A. J.; Cammi, R.; Pomelli, C.; Martin, R. L.; Morokuma, K.; Zakrzewski, V. G.; Salvador, P.; Dannenberg, J. J.; Dapprich, S.; Farkas, J. B.; Foresman, J. V.; Ortiz, J. C.; Fox, D. J. *Gaussian 09*, revision B.01; Gaussian, Inc.: Wallingford, CT, 2010.
(33) Zerner, M. C.; Loew, G. H.; Kirchner, R. F.; Mueller-Westerhoff, U. T. *J. Am. Chem. Soc.* **1980**, *102*, 589−599.
(34) Wu, Z.; Petzold, A.; Henze, T.; Thurn-Albrecht, T.; Lohwasser, R. H.; Sommer, M.; Thelakkat, M. *Macromolecules* **2010**, *43*, 4646−4653.
(35) Brinkmann, M.; Rannou, P. *Adv. Funct. Mater.* **2007**, *17*, 101−108.
(36) Kayunkid, N.; Uttiya, S.; Brinkmann, M. *Macromolecules* **2010**, *43*, 4961−4967.
(37) Kohn, P.; Rong, Z.; Scherer, K. H.; Sepe, A.; Sommer, M.; Müller-Buschbaum, P.; Friend, R. H.; Steiner, U.; Hüttner, S., submitted.
(38) Clark, J.; Silva, C.; Friend, R.; Spano, F. *Phys. Rev. Lett.* **2007**, *98*, 1−4.
(39) Vandewal, K.; Tvingstedt, K.; Gadisa, A.; Inganäs, O.; Manca, J. V. *Phys. Rev. B* **2010**, *81*, 1−8.
(40) Vandewal, K.; Gadisa, A.; Oosterbaan, W. D.; Bertho, S.; Banishoeib, F.; Van Severen, I.; Lutsen, L.; Cleij, T. J.; Vanderzande, D.; Manca, J. V. *Adv. Funct. Mater.* **2008**, *18*, 2064−2070.
(41) Benson-Smith, J. J.; Goris, L.; Vandewal, K.; Haenen, K.; Manca, J. V.; Vanderzande, D.; Bradley, D. D. C.; Nelson, J. *Adv. Funct. Mater.* **2007**, *17*, 451−457.
(42) Jespersen, K. G.; Beenken, W. J. D.; Zaushitsyn, Y.; Yartsev, A.; Andersson, M.; Pullerits, T.; Sundström, V. *J. Chem. Phys.* **2004**, *121*, 12613−7.
(43) Vandewal, K.; Tvingstedt, K.; Gadisa, A.; Inganäs, O.; Manca, J. V. *Nat. Mater.* **2009**, *8*, 904−9.
(44) Huang, Y.; Westenhoff, S.; Avilov, I.; Sreearunothai, P.; Hodgkiss, J. M.; Deleener, C.; Friend, R. H.; Beljonne, D. *Nat. Mater.* **2008**, *7*, 483−9.
(45) Albert-Seifried, S.; Friend, R. H. *Appl. Phys. Lett.* **2011**, *98*, 223304.
(46) Cornil, J.; Gueli, I.; Dkhissi, A.; Sancho-Garcia, J. C.; Hennebicq, E.; Calbert, J. P.; Lemaur, V.; Beljonne, D.; Brédas, J. L. *J. Chem. Phys.* **2003**, *118*, 6615.
(47) Van Vooren, A.; Kim, J.-S.; Cornil, J. *ChemPhysChem* **2008**, *9*, 989−93.
(48) Oberhumer, P. M.; Huang, Y.-S.; Massip, S.; James, D. T.; Tu, G.; Albert-Seifried, S.; Beljonne, D.; Cornil, J.; Kim, J.-S.; Huck, W. T. S.; Greenham, N. C.; Hodgkiss, J. M.; Friend, R. H. *J. Chem. Phys.* **2011**, *134*, 114901.